HHS Public Access

Author manuscript

J Biomater Sci Polym Ed. Author manuscript; available in PMC 2017 January 01.

Published in final edited form as:

J Biomater Sci Polym Ed. 2017 January ; 28(1): 15–32. doi:10.1080/09205063.2016.1239947.

A Chemical Stability Study of Trimethylsilane Plasma Nanocoatings for Coronary Stents

John Eric Jones[1], **Qingsong Yu**[1,*], and **Meng Chen**[2,*]

[1]Center for Surface Science and Plasma Technology, Department of Mechanical & Aerospace Engineering, University of Missouri, Columbia, Missouri 65211, USA

[2]Nanova, Inc., Columbia, Missouri 65211, USA

Abstract

In this study, trimethylsilane (TMS) plasma nanocoatings were deposited onto 316L stainless steel coupons in direct current (DC) and radio frequency (RF) glow discharges and additional NH_3/O_2 plasma treatment to tailor the coating surface properties. The chemical stability of the plasma nanocoatings were evaluated after 12 week (~3 month) storage under dry condition (25 °C) and immersion in simulated body fluid (SBF) at 37 °C. It was found that nanocoatings did not impact surface roughness of underlying stainless steel substrates. X-ray photoelectron spectroscopy (XPS) and Fourier transform infrared spectroscopy (FTIR) were used to characterize surface chemistry and compositions. Both DC and RF TMS plasma nanocoatings had Si– and C– rich composition; and the O– and N– contents on the surfaces were substantially increased after NH_3/O_2 plasma treatment. Contact angle measurements showed that DC TMS nanocoating with NH_3/O_2 treatment generated very hydrophilic surfaces. DC TMS nanocoatings with NH_3/O_2 treatment showed minimal surface chemistry change after 12 week immersion in SBF. However, nitrogen functionalities on RF-TMS coating with NH_3/O_2 post treatment were not as stable as in DC case. Cell culture studies revealed that the surfaces with DC coating and NH_3/O_2 post treatment demonstrated substantially improved proliferation of endothelial cells over the 12 week storage period at both dry and wet conditions, as compared to other coated surfaces. Therefore, DC nanocoatings with NH_3/O_2 post treatment may be chemically stable for long-term properties, including shelf-life storage and exposure to the bloodstream for coronary stent applications.

Keywords

stents; stainless steel; surface modification; ageing; nanocoatings

1. Introduction

In the 1970s, balloon angioplasty was developed as a treatment for occluded coronary arteries [1]. Coronary arteries are essential for supplying oxygen to cardiac tissue. During balloon angioplasty, a balloon catheter is inserted into the femoral artery, guided through the aorta, and into the coronary arteries. The balloon is expanded at the site of the blockage,

*Correspondence to: Q. S. Yu; yuq@missouri.edu, or M. Chen; mengchen2002slc@yahoo.com.

resulting in the opening of the artery and enhanced blood flow [2]. Despite the restored blood flow from balloon angioplasty, there are major drawbacks to this technique. Expanded arteries are subject to elastic recoil, thrombosis, and pooling of blood within the arterial wall. Restenosis is common and develops within six months of angioplasty in the range of 40% [3]. Restenosis is due to injury of the arterial lining caused by balloon expansion. Smooth muscle cells, which are critical to the inflammatory response, aggregate within the treated section, resulting in subsequent blockage of the artery and neointimal hyperplasia [4–6].

Stenting developed as a complement to balloon angioplasty. The first metallic stents were developed by Dr. Palmaz in 1985 [7]. Today, most stents are composed of 316L stainless steel, nitinol, or cobalt chromium [8–10]. Stents are normally placed onto a catheter balloon and inserted within the coronary artery. Upon expansion of the balloon, the stent is positioned within the artery and left in place. Stenting results in a rigid framework that maintains arterial patency. Thus, elastic recoil of the artery is substantially reduced. Short-term complications are minimized, although thrombosis still occurs in 1–3% of patients shortly after implantation [11]. Unfortunately, restenosis still occurs within 20–30% of patients six months post-implantation [12]. This restenosis is likely an immunological reaction due to irritation of the vasculature after expansion [13].

One promising material that has been investigated for the prevention of in-stent restenosis is the drug-eluting stent (DES). DES typically incorporate paclitaxel or sirolimus drugs embedded within a degradable polymer matrix [14, 15]. Over the life of the patient, the coating dissolves, gradually releasing the drug compound. The compounds act on different aspects of cell cycle or structure. Sirolimus inhibits DNA replications, thereby halting cell reproduction [16, 17]. Paclitaxel stabilizes microtubule assembly during cell reproduction. Stable microtubules do not degrade during physical cell division, preventing the formation of daughter cells [16, 18]. Sirolimus and paclitaxel act on the smooth muscle cells, halting their proliferation on the stent and hindering restenosis [19]. Unfortunately, DES can fail to halt late-term restenosis at least six months following implantation [20, 21]. Furthermore, drug compounds may hinder endothelial cell attachment, disrupting the formation of an endothelial lining [16].

Additional coatings have been investigated for their abilities to hinder restenosis. Gold, graphite, diamond, and fluoropolymer-based stent coatings have been actively investigated. Gold has been found to hinder platelet aggregation with respect to other coating methods [22]. However, gold is poorly effective at preventing smooth muscle cell growth [23, 24]. Graphitic coatings have been shown to minimize inflammation compared to gold, yet graphite is more heavily prone to thrombus formation [22]. Diamond-like coatings (DLC) have been found to minimize corrosion and potential platelet activation *in vitro* and *in vivo* [25, 26]. Unfortunately, clinical evaluations have shown that DLC on vascular stents does not effectively mitigate restenosis [25]. Fluoropolymer-based coatings have also been investigated for restenosis mitigation. Fluoropolymer coatings appear to be highly promising as they were found to substantially reduce smooth muscle cell attachment while also promoting endothelialization [27, 28].

Plasma nanocoatings have attracted interest as a biocompatible material because they can be deposited onto many medical devices or implants, highly conformal and pinhole free [29–31], and have excellent adhesion to their substrates even after exposure to mineral-rich physiological medium [32]. With respect to stenting, plasma nanocoatings impart improved corrosion characteristics of the underlying substrate, potentially minimizing inflammation [33]. From an economic standpoint, plasma processes are inexpensive; and treatment/deposition gases are non-toxic [29, 34]. Furthermore, deposition times can be minimized, especially when the substrate serves as cathode [35]. Cathodic deposition can be easily obtained for electrically conductive substrates, including cardiovascular stents made of metals or alloys.

The stability of functionality created on the surface of biomaterials by plasma coating technology is very critical to its successful application for coronary stents. It would need to provide a long-lasting bioactivity on the stent surface. The plasma coating also has to maintain its mechanical integrity since premature delamination or cracking will lessen its benefit. Stability of plasma coatings for biomedical applications has been widely studied through immersing specimens in water or phosphate buffered saline for a certain period of time [36–39]. In this paper, we report on the chemical stability of plasma nanocoatings after prolonged immersion in a simulated body fluid (SBF) at 37 °C. The SBF chosen for this study was Dulbecco's phosphate buffered saline (DPBS). Radio frequency (RF) and direct current (DC) glow discharges were used to deposit 20–30 nm coatings on stainless steel coupons. Trimethylsilane (TMS) was utilized as the coating precursor. TMS nanocoatings were subsequently post-treated using NH_3/O_2 glow discharge plasma. NH_3/O_2 post treatments may produce chemical functionalities that could inhibit restenosis and platelet aggregation [40]. Surface roughness was determined through optical profilometry. Nanocoating surface chemical composition was assessed after SBF immersion using Fourier transform infrared spectroscopy (FTIR) and X-ray photoelectron spectroscopy (XPS). Finally, the biological response of aged coating surfaces was evaluated with 3-day endothelial cell culture test. This study should provide useful information on how the nanocoating composition is potentially affected by the physiological environment.

2. Materials and Methods

2.1. Plasma Nanocoatings Deposited with DC and RF Glow Discharges

Anhydrous ammonia (purity > 99.99%) was provided by Air Liquide (Plumsteadville, PA). Oxygen (purity > 99.6%) was purchased from Airgas (Columbia, MO). TMS (purity > 97%) was supplied by Gelest, Inc. (Morrisville, PA). Cleaned 316L stainless steel coupons (1 cm × 1 cm × 0.1 cm) were utilized for nanocoating deposition, of which surface chemistry and roughness analysis were conducted.

DC glow discharges were created inside an 80 liter bell-jar reactor. Stainless steel coupons were attached to an aluminum holder positioned between two titanium electrodes in parallel. The square titanium electrodes had sides of length 18.2 cm. For all DC treatments, the coupon holder acted as the cathode whereas the two outer titanium electrodes served as the electrically grounded anodes. An oxygen plasma was used to remove organic contaminants on the sample surfaces and provide a controllable fresh surface for the subsequent coating

deposition. The reactor was sealed and evacuated to a base pressure of 1 mTorr using a pump group consisting of mechanical and booster pumps connected in series. Oxygen was then introduced to the reactor at a flow rate of 1 sccm (standard cubic centimeters per minute) using an MKS mass flow controller (MKS Instruments, Andover, MA) and an MKS 247C readout to set the flow rate. The pressure inside the plasma reactor was allowed to stabilize at 50 mTorr using an MKS pressure controller. The oxygen was then excited with the DC power supply at 20 W (watt) to form the plasma. The treatment time was 2 min. Following surface cleaning by O_2 plasma, the reactor was evacuated to a base pressure of 1 mTorr and TMS was introduced to the reactor at 1 sccm. The reactor pressure was allowed to reach 50 mTorr, and the TMS was excited by the DC power supply at 5 W for 15 seconds.

For samples with plasma coating requiring additional surface modification, the reactor was again evacuated to a base pressure of 1 mTorr and the treatment gases were then introduced. The gas composition used in the post surface modification step was a mixture of NH_3 plus O_2 at a ratio of 2:1, because our previous optimization results indicated that this composition could provide improved surface biological responses. The gas composition was maintained by using mass flow rates of 2 sccm for NH_3 and 1 sccm for O_2. The pressure was allowed to equilibrate at 50 mTorr, and the plasma was induced by applying 5 W DC power. The duration of this surface modification process was 2 min.

The gas mixtures used to sustain the DC glow discharge (DCGD) for surface treatments were also employed in the case of RF glow discharge (RFGD) generated by a 13.56 MHz RF power source (RFX-600, Advanced Energy Industries, Inc., Fort Collins, CO). In the arrangement for RF plasma surface treatment and coating deposition, the aluminum frame with the stainless steel coupons to be coated was placed between two active electrodes. In contrast to the DC case, the frame was maintained at a floating potential versus the electrodes. The oxygen plasma pretreatment step was carried out at a power of 20 W RF and a mass flow of 1 sccm for 2 min. Following the treatment, the samples were coated with the TMS plasma coating deposited at 30 W RF for 5 min. One of the RF plasma coated groups was further modified with NH_3/O_2 mixture plasma at 20 W RF for 2 min. All those steps were carried out at a working pressure of 50 mTorr.

2.2. Surface Morphologies of Plasma Nanocoatings

Surface roughness parameters were obtained using an optical profilometer (Wyko NT9100, Veeco Instruments, Inc., New York, NY) with Vision (version 4.10) for data analysis. Stainless steel coupons were mounted horizontally. The scan area was a rectangular spot with approximate dimensions of 125 μm × 94 μm. Scan resolution was 500 nm laterally and 0.5 nm vertically. Collected data were processed after application of a tilt correction. From the data, the arithmetic mean of the absolute values of the vertical dimensions (R_a) and root mean square roughness (R_q) were obtained.

2.3. Contact Angle Measurements of Nanocoated Stainless Steel Surfaces

Surface contact angles were measured using a 1 μl droplet of distilled water dropped onto the substrate surface, and a computer-aided VCA 2500 XE Video Contact Angle System (AST Products, Inc., Billerica, MA). Surface wettability changes over time after plasma

treatment were evaluated by taking surface contact angle measurements over a 12 week period following removal of the coupons from the bell-jar reactor. Throughout the testing period, samples were stored inside glass vials at 25 °C.

A further storage treatment utilized simulated body fluid (SBF) under physiological condition over an immersion time of 12 weeks. The 1 × 1 cm stainless steel coupons were immersed in 1 ml Dulbecco's phosphate buffered saline (DPBS) inside a 24 well plate. Samples were stored inside an incubator held at 37 °C. DPBS was replaced every 2–3 days. On removal from SBF, samples were rinsed twice with distilled water and dried inside a desiccator for 6 hours prior to contact angle analysis.

2.4. Surface Chemical Analysis of Nanocoatings under Dry and Wet Storage

X-ray photoelectron spectroscopy (XPS) was used to determine surface chemical composition of coated stainless steel coupons. A Kratos AXIS 165 X-ray Photoelectron Spectrometer (Kratos Analytical Inc., Chestnut Ridge, NY) utilizing a monochromatic Al Kα X-ray (1486.6 eV) source operating at 150 W was utilized to characterize the coatings to a depth of about 10 nm. The X-ray source take-off angle was set at 90° relative to the coupon surface, and the spot size was about 200 μm × 200 μm.

Fourier transform infrared spectroscopy (FTIR) was carried out in order to determine chemical groups within plasma nanocoatings. FTIR was conducted using a Cary 660 FTIR spectrometer (Agilent Technologies, Santa Clara, CA). Scans were carried out from 4000 to 500 cm^{-1}.

Similar to surface contact angle analysis, dry storage (25 °C) and physiological immersion in DPBS (37 °C) were utilized for nanocoated stainless steel coupons of 1 × 1 cm. The coupons were analyzed via FTIR after drying inside a desiccator for 6 hours.

2.5. Cell Culture Test on Aged Substrates with Nanocoatings

Porcine coronary artery endothelial cells (PCAEC) were acquired from Genlantis (San Diego, CA) at second passage. PCAEC culture medium was also acquired from Genlantis. Culture medium was supplemented with serum and antibiotics by the supplier. Cells were grown inside a 75 cm^2 tissue culture flask in 20 ml medium. Culture medium was replaced every 2 days. When PCAEC became 60% confluent, medium volume was increased to 40 ml. Cells were passaged as soon as they became 80% confluent. Cells were passaged using a subculture kit provided by the cell supplier. Briefly, cells were rinsed with HEPES-buffered saline solution, and trypsinized with the company-supplied trypsin/EDTA solution. Once the cells were detached from the flask surface, trypsin neutralization solution was added to inhibit further trypsin activity. The flask cell suspension was transferred to a 50 ml tube and centrifuged at 200 g for 5 min. The supernatant was aspirated off, and the resulting cell pellet was resuspended in 5 ml culture medium. Cells were counted with a hemocytometer and concentration adjusted to 5×10^4 cells/ml in culture medium.

Nanocoated stainless steel coupons (1 × 1 cm) were either left in glass petri dish with covered lid at room temperature (25 °C, dry storage) or immersed in 1 ml DPBS (37 °C, 5% CO_2, humidified atmosphere). In immersion study, DPBS was replaced every two days.

After 4, 8, and 12 week storage times at both dry and wet conditions, the stainless steel coupons were rinsed with 1 ml culture medium. PCAEC were added to the coupons at 5 $\times 10^4$ cells per ml. Samples were placed inside an incubator (37 °C, 5% CO_2, humidified) for three days. Culture medium was replaced after two days inside incubator.

An MTT assay [41–43] was performed to determine relative cell viabilities of the nanocoatings. After cell incubation, medium was removed and the cells rinsed with DPBS. MTT reagent (Sigma-Aldrich, St. Louis, MO) was dissolved in Dulbecco's Modified Eagle Medium (high glucose, without phenol red) at a concentration of 0.5 mg/ml. One ml MTT solution was added to each well containing coupons. Samples were further incubated for three hours at 37 °C, 5% CO_2, humidified atmosphere. After three hours, MTT medium was removed, and the purple formazan crystals were dissolved in dimethyl sulfoxide (DMSO). The solution absorbance was measured using a microplate reader at 570 nm. The absorbance values correspond to relative cell viabilities.

3. Results and Discussion

3.1. Surface Morphologies of Plasma Nanocoatings on Stents

Plasma nanocoating chemistries could be substantially different from the bare metal substrate. Alterations in surface chemistries likely affect the interactions of material surface with host tissue. However, surface morphology may play an important factor in how cells attach to the substrate. Plasma nanocoatings can be tuned to have topographies that mimic the underlying substrate. Shen et al [44] applied nanocoatings (< 50 nm) to nitinol substrates in order to improve the attachment of endothelial cells *in vitro*. The nanocoatings used by the researchers utilized TMS or TMS+O_2 mixtures in the deposition process. Such coatings had surface roughness values similar to the nitinol substrates. Enhanced adhesion and proliferation of endothelial cells were therefore attributed to the surface chemistries of the nanocoating.

A summary of R_a and R_q values for uncoated and plasma nanocoated stainless steel coupons appears in Figure 1. Roughness parameters are shown for as-deposited nanocoatings from DC and RF power supplies (designated as DC-TMS and RF-TMS, respectively) and NH_3+O_2 modifications from DC and RF (DC-TMS + NH_3/O_2 and RF-TMS + NH_3/O_2, respectively). Those R_a and R_q values provide quantitative information about the surface morphology of nanocoatings and stainless steel substrates. It is indicated that all plasma conditions produced coatings with similar morphologies to bare stainless steel. Therefore, any alterations to stent surface-tissue interactions are more likely to result from surface chemical changes rather than roughness.

3.2. Water Contact Angle Analysis

Figure 2 depicts the surface contact angle measurement results using stainless steel coupons with and without plasma nanocoatings for both dry storage and DPBS immersion conditions. As shown in Figure 2a (dry storage), DC-TMS and RF-TMS nanocoatings were hydrophobic with initial contact angle approximately 105° after plasma coating deposition while DC-TMS+NH_3/O_2 and RF-TMS+NH_3/O_2 showed higher surface energies indicated

by lower contact angle. RF-TMS + NH_3/O_2 group showed a modest increase in initial surface energy (initial contact angle: 57.1°) as compared to RF-TMS whereas the DC glow discharge plasma (DC-TMS+NH_3/O_2) was able to completely wet the plasma coating surfaces initially. During the aging period when the samples were kept in a glass vial, namely dry storage at 25 °C, the contact angle for the coupons modified with DC-TMS +NH_3/O_2 increased due to hydrophobic recovery commonly seen with plasma modified surfaces; however, the contact angle did not rise above that of bare stainless steel, which is 42° in this case. On the other hand, SBF immersion had a noticeable effect on contact angle for bare metal and other nanocoated samples (Figure 2b). Water contact angle fell to near 0° after 12 weeks (about 3 months) for bare metal groups, which could be attributed to some minerals deposited on the substrate surface from DPBS solution. Contact angles remained nearly constant for RF-TMS group, implying no change in surface property. DC-TMS group showed a decrease in contact angle over the immersion period, indicating some sort of electrolyte/mineral adsorption to the coating surface. For RF-TMS + NH_3/O_2 group, the contact angle rose from 58.3° initially to 106.3° after 12 weeks. Please note that the initial contact angle values for RF-TMS+NH_3/O_2 sample are slightly different in Figure 2a (57.1° ± 1.6°) and Figure 2b (58.3° ± 2.4°). These RF-TMS+NH_3/O_2 contact angle values were measured on two separate samples. As there was no significant difference between these values, separate values were used. At the end of the 12 week immersion period, contact angle is negligibly different between RF-TMS and RF-TMS + NH_3/O_2 groups. Contact angles remained at 0° for NH_3/O_2 samples in DC group for at least 1 week. After 12 weeks, contact angle for DC-TMS + NH_3/O_2 increased to 36.0°, suggestive of hydrophobic recovery of the coating surface.

3.3. FTIR and XPS Stability Analysis

Nitrogen incorporation into the plasma coating can be present in the form of numerous chemical groups. In terms of blood-contacting, nitric oxide (NO) has been seen as an important signaling molecule in regulating smooth muscle cell proliferation and platelet attachment [40, 45]. Enhancing the attachment of NO groups on the surface may provide a method to mitigate in-stent restenosis. It is known that nitric oxide (NO) has potent anti-platelet aggregating activity, and has been widely studied for preventing restenosis and thrombus formation on the surface implantable devices such as stents [46–48].

FTIR is able to detect nitrogen functionalities in the plasma nanocoating (Figure 3), primarily in the form of C=N or nitrite esters (C-O-N=O) (Table 1). The new chemical groups are inert under dry storage, and peak intensities of absorption bands identified in Table 1 remain nearly constant over 12 weeks of dry storage for the 4 plasma coating conditions: DC-TMS, DC-TMS+NH_3/O_2, RF-TMS, and RF-TMS+NH_3/O_2 (Figure 3). Interestingly, NH_3/O_2 modified coatings from DC plasmas show substantial C-O-N=O, as denoted by the large, broad peak at 1228 cm^{-1} (Table 1). The C-O-N=O peak masks the C-H peak (from Si-C-H) that would show up at 1252 cm^{-1}.

Modification of TMS nanocoatings is also obtained with the RF plasma and can be seen with the C=N functionality at 1215 cm^{-1}. The Si-C and Si-O moieties attributed to unmodified TMS plasma coatings are still detected after surface modification with NH_3/O_2

plasma powered by RF supply. It can be concluded that the NH_3/O_2 RF plasma does not modify the nanocoating surface as effectively as the DC condition, based on the formation of NO groups and the surface hydrophilicity as reflected by the contact angle data. For instance, the contact angle for DC-TMS+NH_3/O_2 was 39° vs. 82° for RF-TMS+NH_3/O_2 at week 12 under dry storage condition (Figure 2a). In other words, these FTIR studies corroborate the contact angle measurements. In this case, higher surface energy is expected with the more highly polar nature of coatings treated with the DC plasma of NH_3/O_2. Based on the results of endothelial cell culture testing on aged samples, which will be discussed below, the RF-TMS + NH_3/O_2 condition underperformed its DC counterpart in terms of promoting endothelial cell attachment and growth, suggesting lack of potential therapeutic reservoirs of nitric oxide associated with RF-TMS + NH_3/O_2.

During the coupon immersion period in DPBS, DC-TMS and RF-TMS groups displayed very little change in terms absorbance peak shown in FTIR spectra. Si-C and Si-O-Si functionalities are present at nearly consistent levels (Figure 4). NH_3/O_2-modified groups showed some interesting trends that may be indicative of retention of nitrogen/oxygen-containing functionalities. Specifically, for DC-TMS + NH_3/O_2 group, the peak at 1228 cm^{-1} begins to decline slightly in intensity after one day immersion. After 12 weeks, the nitrogen functionality is still present, yet the C-H peak at 1256 cm^{-1} becomes more easily resolved (Figure 4c). Furthermore, the 36.0° contact angle for the DC-TMS + NH_3/O_2 group after 12 weeks (Figure 2b) lends support that polar functionality remains quite stable. All these observations are in contrast to the RF-TMS + NH_3/O_2 group. For RF post treatment samples, the nitrogen functionality evidenced at 1215 cm^{-1} nearly completely disappeared over the immersion period of 12 weeks. This marked decline in nitrogen functional groups for RF groups is corroborated by the increasing contact angle values in Figure 2b, that is, from the initial 58° to the eventual 106° at week 12. Therefore, NH_3/O_2 modified RF nanocoating groups do not appear to retain the nitrogen functionalities as readily as the modified DC groups.

Further XPS studies were carried out for DPBS-immersed DC-TMS + NH_3/O_2 and RF-TMS + NH_3/O_2 nanocoating groups. Full elemental compositions were obtained for both coating conditions. Both DC-TMS + NH_3/O_2 (Table 2) and RF-TMS + NH_3/O_2 (Table 3) conditions show a decrease in the surface nitrogen concentration over the 12 week immersion period. However, the decrease appears more pronounced with the RF-TMS + NH_3/O_2 condition, as the final surface nitrogen concentration falls to 0.77% after 12 weeks. On the other hand, surface nitrogen concentration is 1.34% after 12 weeks for DC treatment. To account for the differences in elemental composition, N/Si ratios are also shown in Table 2 and Table 3. The N/Si ratio may help control for surface reactions or possible polystyrene contamination, mainly carbon, from the culture wells used for immersion. XPS survey scans provide additional corroborating information regarding contamination and surface stability (Figure 5). It is observed that atomic concentrations of oxygen and nitrogen fall during the SBF immersion period. Carbon content for both DC-TMS + NH_3/O_2 and RF-TMS + NH_3/O_2 coated surfaces rose during the immersion period at the expense of oxygen and nitrogen. For the DC-TMS + NH_3/O_2 treatment, N/Si is highly consistent (~0.1). For RF-TMS + NH_3/O_2 nanocoating conditions, N/Si was initially high at 0.17; however, after 12 week immersion N/Si fell to 0.04. Such a fall in N/Si for the RF-TMS + NH_3/O_2 condition could indicate

insufficient stability of the RF coating group in terms of nitrogen group preservation. Both FTIR and XPS data confirm the loss of nitrogen functionality for RF coating condition. Thus, thus specific RF condition utilized in this study may not be suitable for producing coatings with needed stability within the blood.

Substantial mineral uptake was noted for DC-TMS + NH_3/O_2 nanocoatings immersed in DPBS. After 1 week immersion, sodium, chloride and phosphorus concentrations peaked at 6.59%, 2.15%, and 1.64%, respectively. After 12 week immersion time, sodium content was negligible on DC-TMS + NH_3/O_2 surface with no additional minerals detected. The uptake and subsequent loss of mineral from DPBS may be due to the loss of some polar groups from the surface.

The high resolution N 1s scans over the immersion period (Figure 6) illustrate the decreasing intensity of the nitrogen peak. High resolution peak assignments for N 1s appear in Table 4. Interestingly, the RF nanocoating condition shows a homogeneous bonding within the surface region. The peak for the RF condition (399–400 eV) possibly corresponds to C=N [56, 57] and this assignment corroborates the FTIR assignment. DC-TMS + NH_3/O_2 nanocoating condition produces three distinct curves under the N 1s peak. For the DC samples, a low binding energy peak (398 eV) may correspond to C-N bonding [58, 59]. A peak at 400 eV possibly corresponds to C=N structures [60, 61] whereas the higher binding energy peak at 401–402 eV could be associated with C-O-N=O bonding [62–64]. This XPS peak fits nicely with the explanation for the FTIR peak at 1228 cm^{-1}. It can be seen that the C-O-N=O concentrations at day 0, week 2 and week 12 are 26.34%, 18.64%, and 18.11%, respectively, suggesting that the NO groups could become stable at 2 weeks after immersion in SBF although the overall nitrogen concentration decreases over the immersion period of 12 weeks.

3.4. Proliferation of Endothelial Cells on Aged Nanocoatings

Endothelial recovery is an essential component for vascular healing by providing critical structural and anti-thrombogenic functions [28]. Porcine coronary artery endothelial cells were used for the evaluation of endothelialization on stainless steel surfaces with nanocoatings. As known, one of the main problems with stents is a lack of endothelial cell interactions, which if sufficient, would create a uniform healthy endothelium masking the underlying foreign metal from inflammatory cell interference. The lack of complete endothelial coverage of stent struts associated with persistence of fibrin deposits is believed to be the primary pathoanatomic substrate of late stent thrombosis after DES implantation [65]. To evaluate the durability of bioactivity created on the coated surfaces, three-day cell culture tests were performed on coated SS substrates at 4, 8 and 12 weeks after being stored at dry condition and wet condition (in simulated body fluid). The cell culture results (Figure 7) indicated that as compared to other coating conditions, the growth of endothelial cells on SS coupons coated with DC-TMS+NH_3/O_2 were significantly enhanced even at 12 weeks after plasma coating process. These data strongly suggested that a long lasting surface bioactivity enhancing endothelialization could be generated on stents by the functional nanocoatings.

4. Conclusions

TMS plasma nanocoatings were deposited onto 316L stainless steel coupons in DC and RF glow discharges and then were subsequently modified with NH_3/O_2 post-plasma modification. Under dry storage conditions at 25 °C, the coating surface chemistry remained stable over 12 week storage. On immersion in SBF, DC TMS plasma nanocoatings with NH_3/O_2 post treatment retained nitrogen-containing functionalities, postulated to be an immobilized organic nitrite reservoir. RF treated nanocoatings were chemically stable under dry storage, yet nitrogen-containing groups were depleted over 12 week immersion in SBF. Thus, DC-based nanocoatings treated with NH_3/O_2 post treatment may provide a therapeutic reservoir for the prevention of restenosis. These coatings have potential application in preventing restenosis and platelet aggregation on cardiovascular stents.

Acknowledgments

The authors are grateful to the National Heart, Lung, and Blood Institute (NHLBI) of the National Institutes of Health (NIH) for financial support to this research under Award Number R44HL097485. We also wish to thank Brian Porter at Material Science Center, Missouri University of Science and Technology for his help in the XPS data analysis of the substrates.

References

1. Steele PM, Chesebro JH, Stanson AW, Holmes DR Jr, Dewanjee MK, Badimon L, Fuster V. Circ Res. 1985; 57105
2. Fischell TA, Derby G, Tse TM, Stadius ML. Circulation. 1988; 78:1323. [PubMed: 2973376]
3. Levine GN, Chodos AP, Loscalzo J. Clin Cardiol. 1995; 18:693. [PubMed: 8608668]
4. Borst C. Laser Med Sci. 1987; 2:137.
5. Jawien A, Bowen-Pope DF, Lindner V, Schwartz SM, Clowes AW. J Clin Invest. 1992; 89:507. [PubMed: 1531345]
6. Wiedermann JG, Marboe C, Amols H, Schwartz A, Weinberger J. J Am Coll Cardiol. 1994; 23:1491. [PubMed: 8176112]
7. Noeldge G, Richter GM, Roessle M, Haag K, Katzen BT, Becker GJ, Palmaz JC. Cardiovasc Intervent Radiol. 1992; 15:342. [PubMed: 1423396]
8. Thierry B, Merhi Y, Bilodeau L, Trépanier C, Tabrizian M. Biomaterials. 2002; 23:2997. [PubMed: 12069342]
9. Mani G, Feldman MD, Patel D, Agrawal M. Biomaterials. 2007; 28:1689. [PubMed: 17188349]
10. Garg S, Serruys PW. J Am Coll Cardiol. 2010; 56:S1. [PubMed: 20797502]
11. Eltchaninoff H, Koning R, Tron C, Gupta V, Cribier A. J Am Coll Cardiol. 1998; 32:980. [PubMed: 9768721]
12. De Jaegere P, Mudra H, Figulla H, Almagor Y, Doucet S, Penn I, Colombo A, Hamm C, Bartorelli A, Rothman M, Nobuyoshi M, Yamaguchi T, Voudris V, DiMario C, Makovski S, Hausmann D, Rowe S, Rabinovich S, Sunamura M, Van Es GA. Eur Heart J. 1998; 19:1214. [PubMed: 9740343]
13. Bhargava B, Karthikeyan G, Abizaid AS, Mehran R. Brit Med J. 2003; 327:274. [PubMed: 12896943]
14. Pires NMM, Eefting D, De Vries MR, Quax PHA, Jukema JW. Heart. 2007; 93:922. [PubMed: 17449502]
15. Wessely R, Schömig A, Kastrati A. J Am Coll Cardiol. 2006; 47:708. [PubMed: 16487832]
16. Oberhoff M, Herdeg C, Baumbach A, Karsch KR. Catheter Cardio Inte. 2002; 55:404.
17. Javier AF, Bata-Csorgo Z, Ellis CN, Kang S, Voorhees JJ, Cooper KD. J Clin Invest. 1997; 99:2094. [PubMed: 9151781]

18. Giannakakou P, Sackett DL, Ward Y, Webster KR, Blagosklonny MV, Fojo T. Nat Cell Biol. 2000; 2:709. [PubMed: 11025661]
19. Kastrati A, Mehilli J, Von Beckerath N, Dibra A, Hausleiter J, Pache J, Schühlen H, Schmitt C, Dirschinger J, Schömig A. J Amer Med Assoc. 2005; 293:165.
20. Liistro F, Colombo A. Heart. 2001; 86:262–264. [PubMed: 11514475]
21. Feres F, Costa JR Jr, Abizaid A. Catheter Cardio Inte. 2006; 68:83.
22. Sprague EA, Palmaz JC. J Endovasc Ther. 2005; 12:594. [PubMed: 16212461]
23. Kastrati A, Schömig A, Dirschinger J, Mehilli J, Von Welser N, Pache J, Schühlen H, Schilling T, Schmitt C, Neumann F-J. Circulation. 2000; 101:2478. [PubMed: 10831521]
24. Wieneke H, Sawitowski T, Wnendt S, Fischer A, Dirsch O, Karoussos IA, Erbel R. Herz. 2002; 27:518. [PubMed: 12378397]
25. Roy KR, Lee K-R. J Biomed Mater Res B. 2007; 83B:72.
26. Castellino M, Stolojan V, Virga A, Rovere M, Cabiale K, Galloni MR, Tagliaferro A. Anal Bioanal Chem. 2013; 405:321. [PubMed: 23052887]
27. Gutiérrez-Chico JL, Van Geuns RJ, Regar E, Van Der Giessen WJ, Kelbaek H, Saunamäki K, Escaned J, Gonzalo N, Di Mario C, Borgia F, Nüesch E, García-García HM, Silber S, Windecker S, Serruys PW. Eur Heart J. 2011; 32:2454. [PubMed: 21659439]
28. Chin-Quee SL, Hsu SH, Nguyen-Ehrenreich KL, Tai JT, Abraham GM, Pacetti SD, Chan YF, Nakazawa G, Kolodgie FD, Virmani R, Ding NN, Coleman LA. Biomaterials. 2010; 31:648. [PubMed: 19822362]
29. Chu PK, Chen JY, Wang LP, Huang N. Mat Sci Eng R. 2002; 36:143.
30. Han LM, Timmons RB, Bogdal D, Pielichowski J. Chem Mater. 1998; 10:1422.
31. Steen ML, Flory WC, Capps NE, Fisher ER. Chem Mater. 2001; 13:2749.
32. Weikart CM, Matsuzawa Y, Winterton L, Yasuda HK. J Biomed Mater Res A. 2001; 54:597.
33. Jones JE, Chen M, Yu Q. J Biomed Mater Res B. 2014; 102:1363.
34. Buchgraber C, Spanring J, Pogantsch A, Turner M, Kern W. Synthetic Met. 2004; 147:91.
35. Yu QS, Yasuda HK. Plasmas Polym. 2002; 7:41.
36. Daunton C, Smith LE, Whittle JD, Short RD, Steele DA, Michelmore A. Plasma Process Polym. 2015; 12:817.
37. Lerouge S, Barrette J, Ruiz J-C, Sbai M, Savoji H, Saoudi B, Gauthier M, Wertheimer MR. Plasma Process Polym. 2015; 12:882.
38. Finke B, Schröder K, Ohl A. Plasma Process Polym. 2009; 6:S70.
39. Ruiz J-C, St-Georges-Robillard A, Thérésy C, Lerouge S, Wertheimer MR. Plasma Process Polym. 2010; 7:737.
40. Chen M, Zamora PO, Peña L, Som P, Osaki S. J Biomed Mater Res A. 2003; 67A:994.
41. Liu H, Slamovich EB, Webster TJ. J Biomed Mater Res A. 2006; 78A:798.
42. Vickers NJ, McArthur SL, Shard AG, MacNeil S. Plasma Process Polym. 2008; 5:192.
43. Sardella E, Fisher ER, Shearer JC, Trulli MG, Gristina R, Favia P. Plasma Process Polym. 2015; 12:786.
44. Shen Y, Wang G, Chen L, Li H, Yu P, Bai M, Zhang Q, Lee J, Yu Q. Acta Biomater. 2009; 5:3593. [PubMed: 19477302]
45. Millar TM, Stevens CR, Benjamin N, Eisenthal R, Harrison R, Blake DR. FEBS Lett. 1998; 427:225. [PubMed: 9607316]
46. Reynolds MM, Hrabie JA, Oh BK, Politis JK, Citro ML, Keefer LK, Meyerhoff ME. Biomacromolecules. 2006; 7:987. [PubMed: 16529441]
47. Kushwaha M, Anderson JM, Bosworth CA, Andukuri A, Minor WP, Lancaster JR Jr, Anderson PG, Brott BC, Jun H-W. Biomaterials. 2010; 31:1502. [PubMed: 19913295]
48. Alagem-Shafir M, Kivovich E, Tzchori I, Lanir N, Falah M, Flugelman MY, Dinnar U, Beyar R, Lotan N, Sivan SS. Acta Biomaterialia. 2014; 10:2304. [PubMed: 24389316]
49. Al-Oweini R, El-Rassy H. J Mol Struct. 2009; 919:140.
50. Han LM, Pan J-S, Chen S-M, Balasubramanian N, Shi J, Wong LS, Foo PD. J Electrochem Soc. 2001; 148:F148.

51. Wang MR, Rusli M, Yu B, Babu N, Li CY, Rakesh K. Thin Solid Films. 2004; 462–463:219.
52. Wang J, Pamidi PVA, Zanette DR. J Am Chem Soc. 1998; 120:5852.
53. Chen Q, Yakovlev NL. Appl Surf Sci. 2010; 257:1395.
54. Richter M, Bentrup U, Eckelt R, Schneider M, Pohl M-M, Fricke R. Appl Catal B. 2004; 51:261.
55. Ilharco LM, Garcia AR, Fidalgo AM, Barros R, Vale AF, Da Silva JL, Da Silva AMG. Langmuir. 1995; 11:2745.
56. Lin CH, Chang SL, Hsieh CW, Lee HH. Polymer. 2008; 49:1220.
57. Stapinski T, Swatowska B. J Non-Cryst Solids. 2006; 352:1406.
58. Deng Z-W, Souda R. Diam Relat Mater. 2002; 11:1676.
59. Titantah JT, Lamoen D. Diam Relat Mater. 2007; 16:581.
60. Alexandrescu R, Huisken F, Pugna G, Crunteanu A, Petcu S, Cojocaru S, Cireasa R, Morjan I. Appl Phys A. 1997; 65:207.
61. Dementjev AP, de Graaf A, van de Sanden MCM, Maslakov KI, Naumkin AV, Serov AA. Diam Relat Mater. 2000; 9:1904.
62. Shui M, Zhao Z, Cheng K, Xiong Y, Wu Y, Fan W, Yu J, Yan Y, Yang Z, Gu Y, Zhong F, Xu T. Optik. 2013; 124:6115.
63. Owens FJ, Sharma J. J Appl Phys. 1980; 51:1494.
64. Ren Z-M, Ying Z-F, Du Y-C, Li F-M, Lin J, Ren Y-Z, Zong X-F. Tribol Lett. 1998; 5:141.
65. Joner M, Finn AV, Farb A, Mont EK, Kolodgie FD, Ladich E, Kutys R, Skorija K, Gold HK, Virmani R. J Am Coll Cardiol. 2006; 48:193. [PubMed: 16814667]

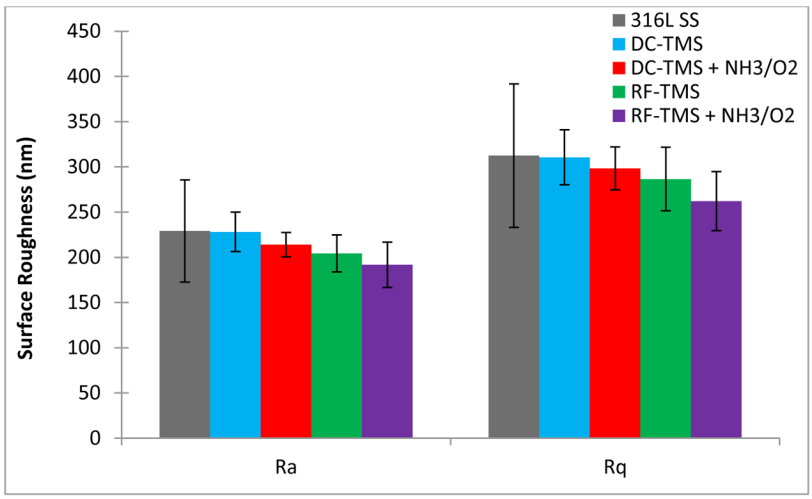

Figure 1.
Surface roughness parameters (R_a and R_q) for uncoated and plasma nanocoated stainless steel.

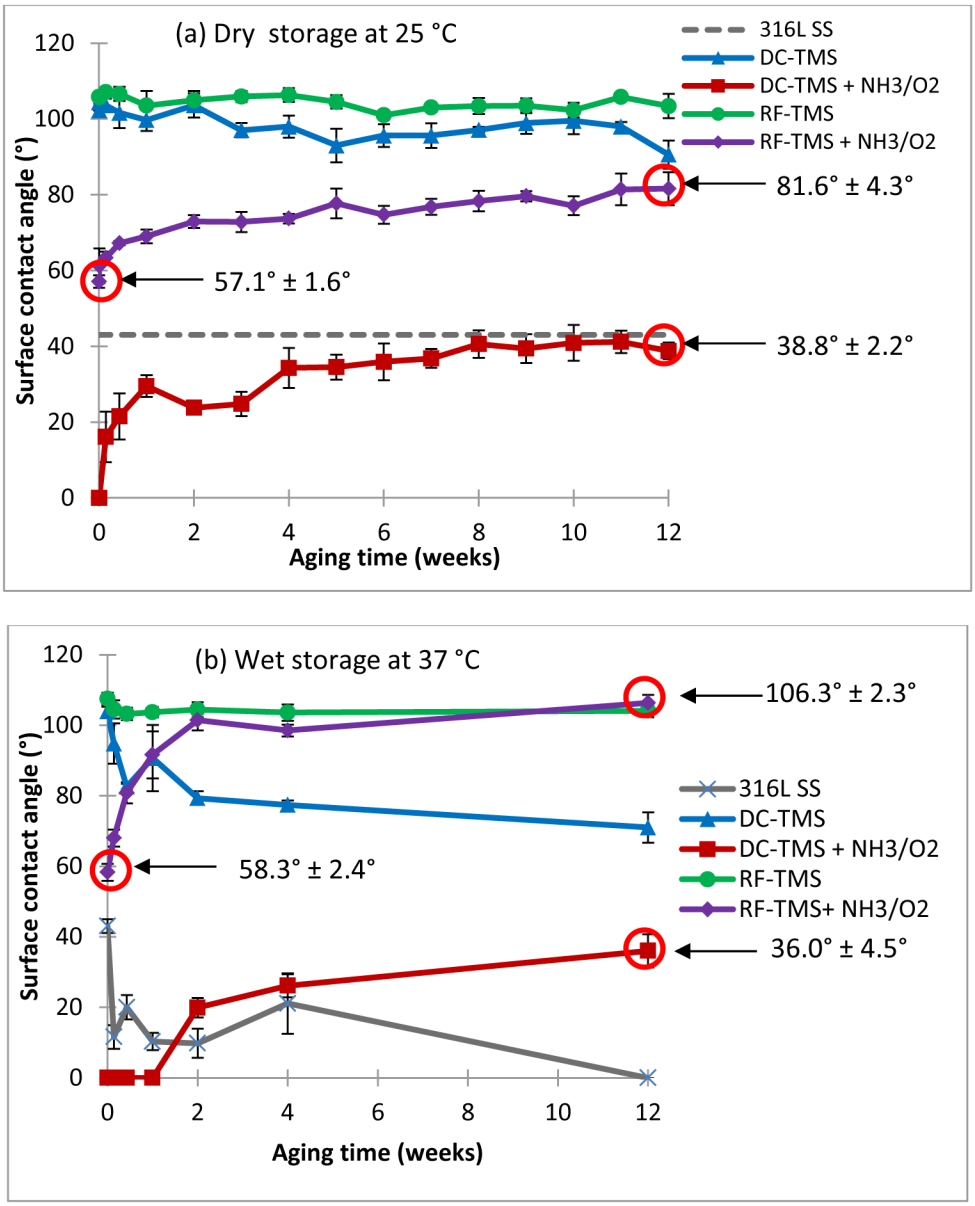

Figure 2.

Surface contact angle measurements of plasma coating deposited onto 316L stainless steel (SS) coupons. 316L SS, uncoated stainless steel; DC-TMS: TMS plasma coating using DC power supply; DC-TMS + NH_3/O_2: TMS plasma coating followed by additional NH_3/O_2 plasma surface modification using DC power supply; RF-TMS: TMS plasma coating using RF power supply; and RF-TMS + NH_3/O_2: TMS plasma coating followed by additional NH_3/O_2 plasma surface modification using RF power supply. Samples were measured under both dry storage and after immersion in simulated body fluid (SBF).

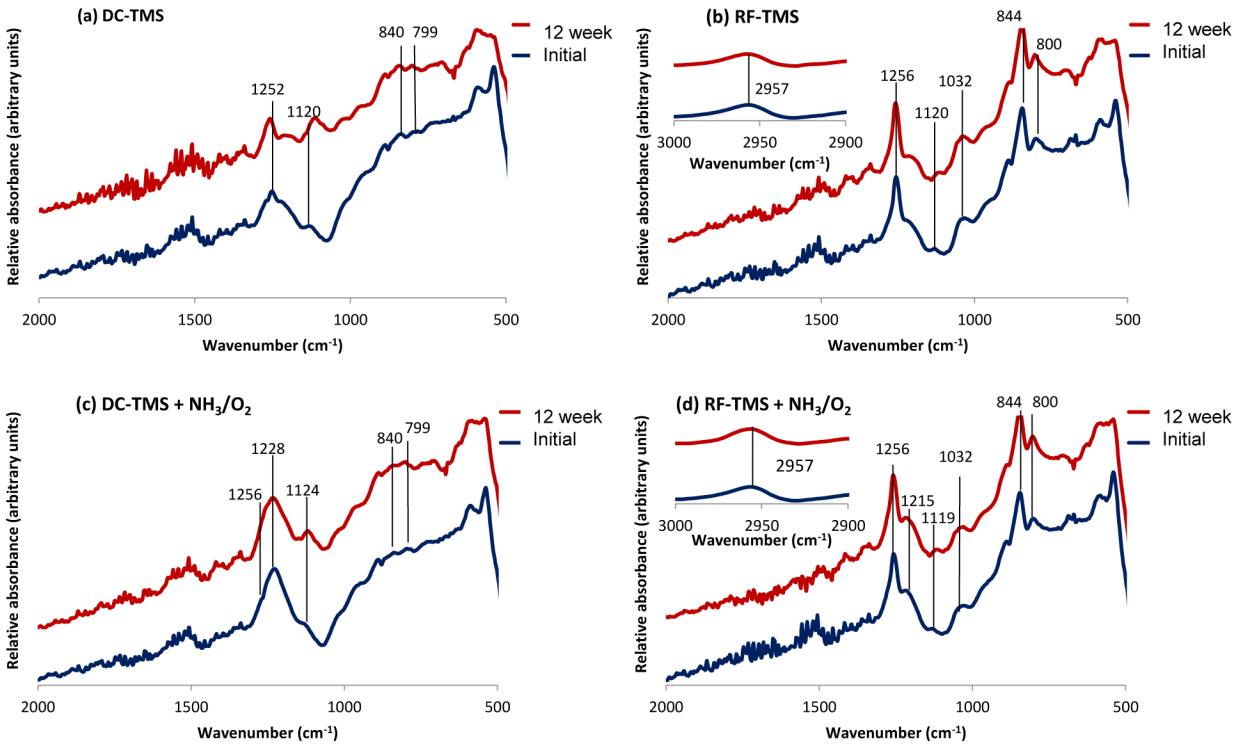

Figure 3.

FTIR spectra for plasma nanocoatings under various coating and treatment conditions through 12 week dry storage (25 °C).

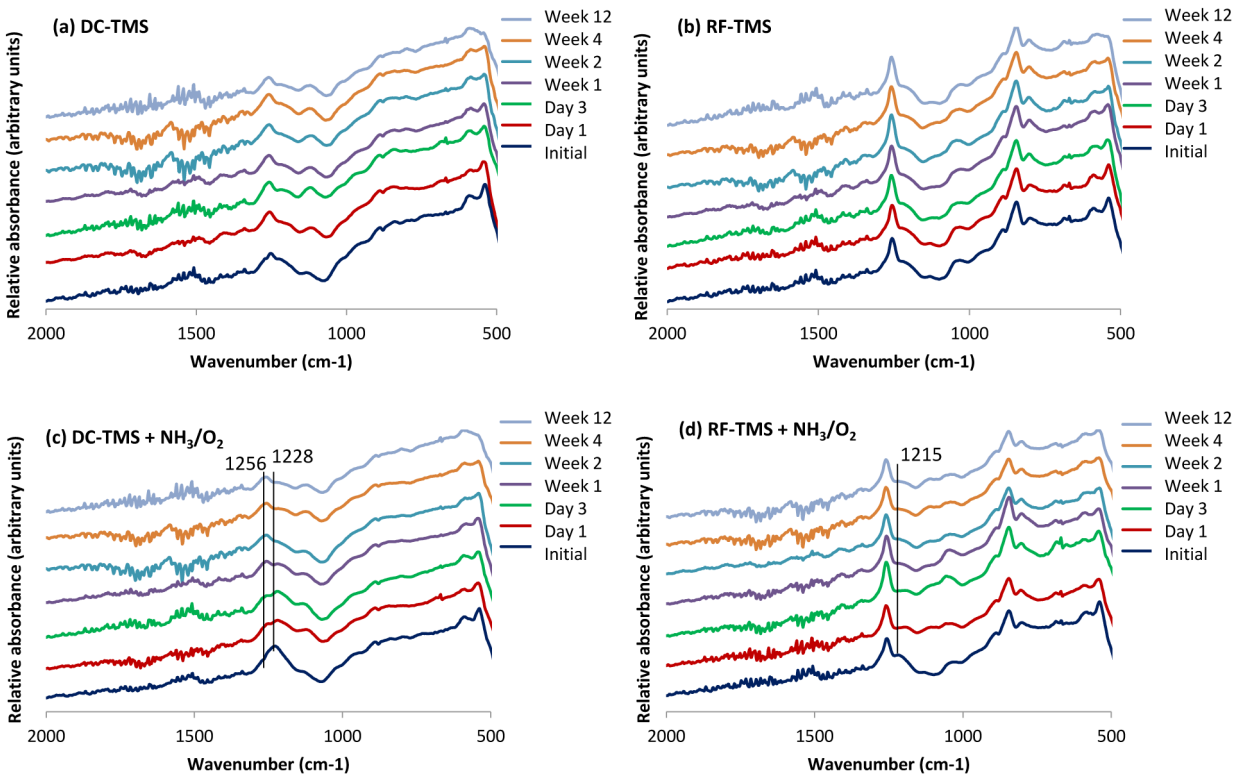

Figure 4.

FTIR spectra for nanocoated specimens after immersion in SBF for various durations at 37 °C.

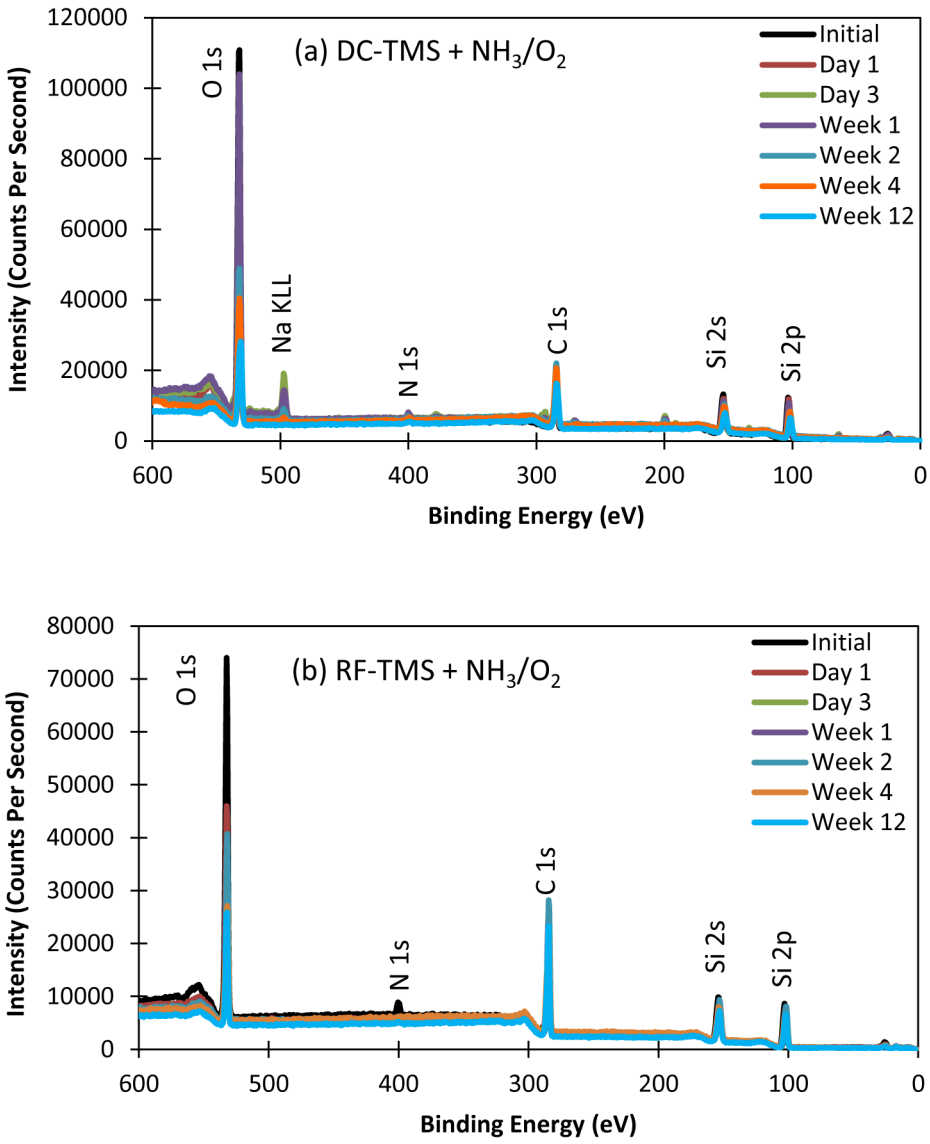

Figure 5.

XPS survey spectra for nanocoated DC-TMS + NH_3/O_2 and RF-TMS + NH_3/O_2 plasma groups after immersion in SBF for various durations at 37 °C.

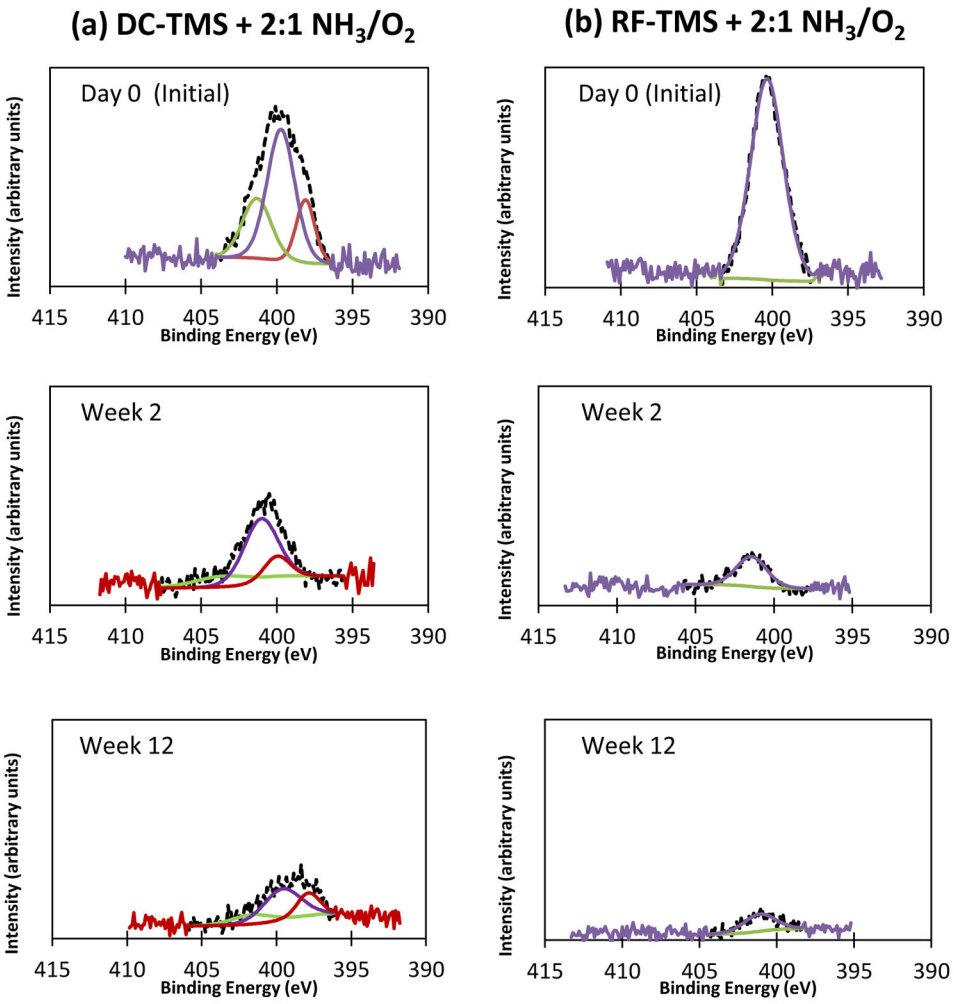

Figure 6.

High resolution scans of the N 1s peaks for DC-TMS + NH_3/O_2 and RF-TMS + NH_3/O_2 plasma groups after immersion in SBF for various durations at 37 °C.

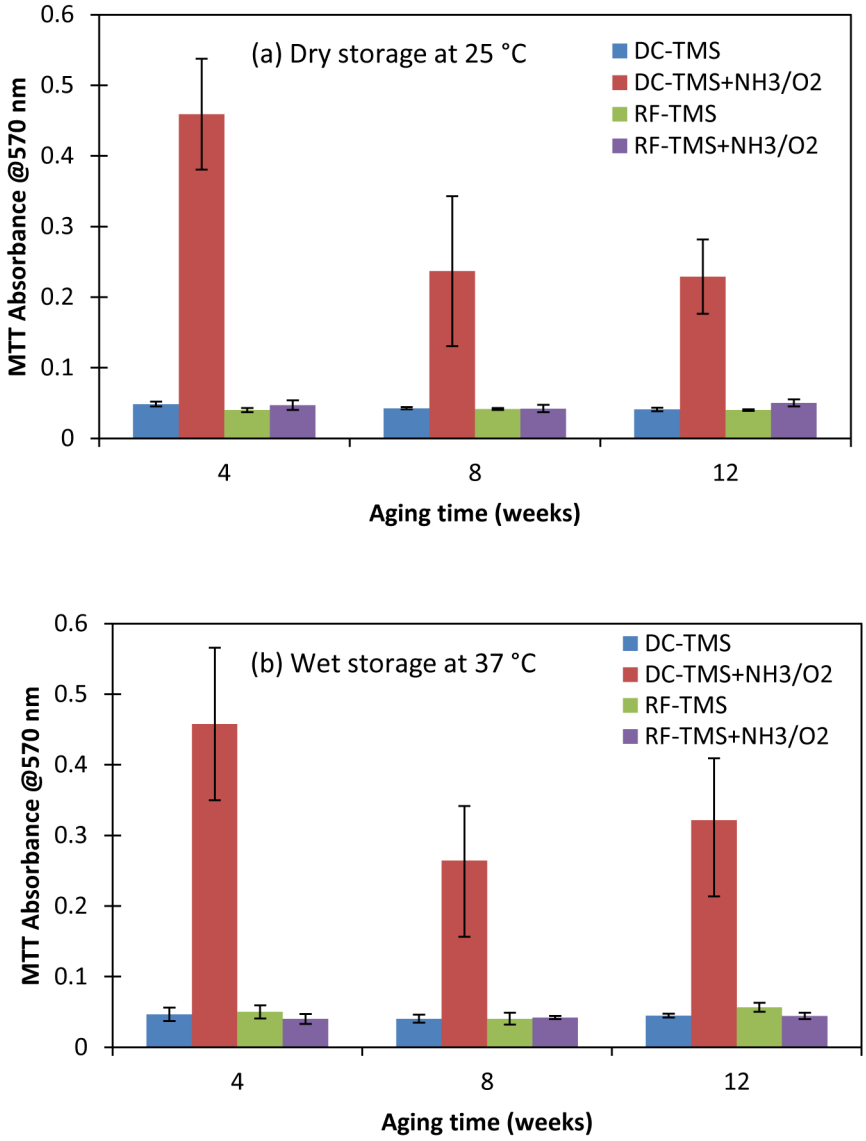

Figure 7.

Growth of endothelial cells at day 3 post cell seeding on the surfaces with nanocoatings aged over a period of 12 weeks at dry condition (a) and wet condition (b).

Table 1

FTIR peak assignments for plasma nanocoatings

Power supply	Wavenumber (cm^{-1})	Peak assignment
DC	1252, 1256	C-H (in Si-C-H) [49]
	1120, 1124	Si-O (in Si-O-Si) [49–53]
	1228	C-O-N=O [54]
	840	Si-C [49]
	799	Si-O (in Si-O-Si) [49]
RF	2957	CH_3 [55]
	1256	C-H (in Si-C-H) [49]
	1215	C=N [56]
	1120	Si-O (in Si-O-Si) [50–53]
	1032	CH_2 [57]
	844	Si-C [49]
	800	Si-O (in Si-O-Si) [49]

Table 2

Surface elemental concentrations for DC-TMS + NH_3/O_2 over 12-week immersion period from XPS (atomic %)

Immersion time	C	Si	O	N	Na	Cl	Al	Zn	K	P	Ti	Fe	*N/Si**
Day 0	16.54	21.38	59.54	2.41	0.13	0.00	0.00	0.00	0.00	0.00	0.00	0.00	***0.11***
Day 1	23.90	18.15	52.59	2.63	1.69	0.00	1.04	0.00	0.00	0.00	0.00	0.00	***0.14***
Day 3	22.58	15.72	51.98	1.68	5.05	1.27	0.63	0.12	0.45	0.52	0.00	0.00	***0.11***
Week 1	28.83	12.84	44.58	1.21	6.59	2.15	0.85	0.00	1.24	1.64	0.07	0.00	***0.09***
Week 2	44.77	16.45	33.26	1.76	2.23	1.27	0.00	0.00	0.00	0.00	0.00	0.26	***0.11***
Week 4	46.75	19.36	31.24	1.68	0.97	0.00	0.00	0.00	0.00	0.00	0.00	0.00	***0.09***
Week 12	49.18	19.17	30.31	1.34	0.00	0.00	0.00	0.00	0.00	0.00	0.00	0.00	***0.07***

* denotes ratio of N-to-Si within surface region

J Biomater Sci Polym Ed. Author manuscript; available in PMC 2017 January 01.

Table 3

Surface elemental concentrations for RF-TMS + NH_3/O_2 over 12-week immersion period from XPS (atomic %)

Immersion time	C	Si	O	N	Na	Cl	*N/Si**
Day 0	35.58	19.29	41.74	3.31	0.08	0.00	***0.17***
Day 1	47.61	19.74	31.24	0.68	0.38	0.35	***0.03***
Day 3	54.65	19.53	24.14	1.68	0.00	0.00	***0.09***
Week 1	56.21	20.30	22.35	1.14	0.00	0.00	***0.06***
Week 2	58.24	20.34	20.25	1.10	0.07	0.00	***0.05***
Week 4	57.72	20.16	21.65	0.35	0.12	0.00	***0.02***
Week 12	59.90	20.36	18.97	0.77	0.00	0.00	***0.04***

* denotes ratio of N-to-Si within surface region

Table 4

XPS peak assignments for DC-TMS + NH_3/O_2 nanocoating group after immersion in PBS

Immersion time	Binding energy (eV)	Peak assignment	Relative concentration (%)
Day 0	398.1	C-N	17.87
	399.7	C=N	55.78
	401.3	C-O-N=O	26.34
Week 2	398.3	C-N	17.00
	399.7	C=N	64.36
	401.8	C-O-N=O	18.64
Week 12	396.9	C-N	25.27
	398.7	C=N	56.62
	400.8	C-O-N=O	18.11